Materials Advances

Accepted Manuscript

This article can be cited before page numbers have been issued, to do this please use: K. Sharma, A. Pal, S. Jha and N. Dey, *Mater. Adv.*, 2026, DOI: 10.1039/D6MA00344C.

ROYAL SOCIETY OF CHEMISTRY

rsc.li/materials-advances

View Article Online
DOI: 10.1039/D6MA00344C

Hydrogen-Bonding Mediated Supramolecular Assembly of Fluorescent Meso-Aryl Porphyrins for Creatinine Monitoring in Biological Samples

Karisma Sharma,[a] Animesh Pal,[b] Satadru Jha,[a] Nilanjan Dey[b*]
[a] Department of Chemistry, Sikkim Manipal Institute of Technology,
Sikkim Manipal University, Majitar, Sikkim 737136, India.
[b] Department of Chemistry, BITS-Pilani Hyderabad Campus, Shameerpet, Hyderabad-500078,
Telangana, India, *Email: nilanjandey.iisc@gmail.com

ABSTRACT

Herein, we report the design, synthesis, and mechanistic evaluation of two meso-aryl free-base porphyrins for selective creatinine detection in aqueous and biological media. Probe 1, bearing terminal electron-withdrawing –CN substituents, exhibited superior photostability, reduced aggregation, and stronger emission (λmax = 430 nm) compared to unsubstituted Probe 2 (λmax = 430 nm). Creatinine triggered a dual optical response: Soret-band hypochromicity and far-red fluorescence quenching via hydrogen-bond-driven ground-state complexation, with a binding constant of K_b = 1.25 × 10^4 M^{-1} for Probe 1 and 4.154*10^3 M^{-1} for Probe 2. Microenvironment-controlled spectroscopy, FT-IR, DLS, and SEM confirmed N–H···O/N hydrogen-bonded adducts and aggregate formation as the dominant mechanism. Probe 1 achieved a low limit of detection (LOD = 0.017 μM; 3σ/k) in buffer, enabling semi-quantitative analysis of creatinine (0–50 μM) in diluted human urine with minimal matrix interference. This structurally tunable porphyrinic platform integrates robust optical signatures with biologically relevant recognition, promising point-of-care renal biomarker monitoring.

Keywords: Porphyrins, H-bonding, Fluorescence turn-off, Creatinine, urine, aggregates,

INTRODUCTION

Creatinine holds significant importance in both human health and environmental systems, making its precise monitoring crucial. Physiologically, creatinine is the end-product of creatine phosphate metabolism in skeletal muscles and is generated at a fairly constant rate proportional to muscle mass. [1] It is eliminated mainly through glomerular filtration; hence, its concentration in blood and urine serves as a key diagnostic indicator of renal function. Normal serum creatinine levels typically range from 0.6–1.3 mg/dL in adults, while normal urinary creatinine excretion ranges from 500–2000 mg/day. [2] Deviations from these values are associated with reduced glomerular filtration rate (GFR), early stages of chronic kidney disease (CKD), acute kidney injury (AKI), and drug-induced nephrotoxicity. [3] Environmentally, creatinine is a prevalent nitrogenous organic pollutant in domestic sewage, industrial effluents, and livestock waste. Through microbial degradation, it is converted into ammonia and nitrites, contributing to eutrophication, algal bloom formation, and dissolved oxygen depletion in aquatic systems. [4] Therefore, the development of advanced creatinine sensing platforms, based on mechanisms such as hydrogen-bond-assisted supramolecular recognition, metal–ligand coordination, ICT (intramolecular charge transfer) modulation, fluorescence quenching/enhancement, and enzyme-mimetic catalysis, is vital for achieving high sensitivity and selectivity in complex biological and environmental matrices. Such reliable detection supports improved clinical diagnostics, personalized health monitoring, wastewater treatment management, and overall environmental sustainability. [5]

Porphyrin-based probes have emerged as exceptionally powerful sensing platforms due to their highly tunable π-conjugated macrocyclic framework, rich photophysical properties, and strong

View Article Online
DOI: 10.1039/D6MA00344C

coordination chemistry, making them ideal for biosensing applications such as creatinine detection. [6] Their rigid tetrapyrrolic core supports intense Soret and Q-band absorptions, high molar extinction coefficients, long-lived excited states, and efficient intersystem crossing, enabling sensitive optical readouts through fluorescence, phosphorescence, resonance light scattering, or ratiometric absorption changes. Metalloporphyrins (e.g., Zn-, Ni-, Cu-, or Fe-porphyrins) further enhance selectivity by providing metal centers capable of axial coordination, hydrogen bonding, or Lewis acid–base interactions with target biomolecules.[7] In creatinine sensing, porphyrins exploit specific binding through carbonyl–metal coordination, N–H…N or N–H…π interactions, and pH-responsive protonation–deprotonation of meso-aryl substituents, which modulate electronic transitions and produce distinct spectral shifts. [8] Their ability to self-assemble into J- or H-aggregates in aqueous or micellar media offers additional signal amplification due to excitonic coupling. [9] Here, we have introduced the -CN substituents to increase the electronic density and photophysical properties of the porphyrin core through a strong electron-withdrawing effect, thereby improving solvation and modulating excited-state behaviour. Two -CN groups were selected as a balanced design: enough to influence the electronic structure and sensing response. Thus, the choice reflects a controlled structure–property optimisation rather than an arbitrary substitution pattern. The biocompatibility, structural modularity, and ability to incorporate functional groups or nanomaterial scaffolds allow porphyrin probes to operate efficiently in complex biological fluids, offering nanomolar-level detection, high photostability, and real-time sensing. [10] These attributes position porphyrin-based systems as versatile and robust optical transducers for biosensing platforms targeting clinically relevant analytes such as creatinine, glucose, nitric oxide, bilirubin, and various enzymes, thereby advancing non-invasive diagnostics and point-of-care biomedical technologies. [11]

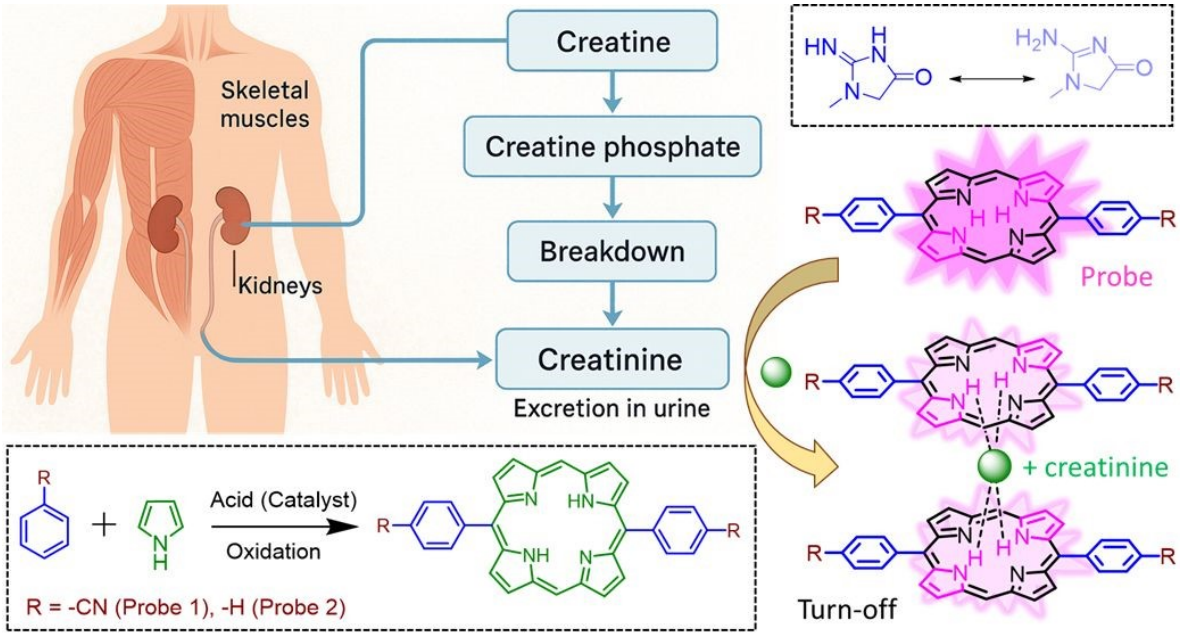

Figure 1. Schematic diagram shows formation creatinine in human body. Design and synthesis of probe molecules (**1**, **2**) for creatinine detection and template mediated co-assembly.

In this context, the present study introduces a structurally tunable porphyrin-based sensing platform that exploits hydrogen-bond–mediated supramolecular recognition to achieve selective and sensitive creatinine detection in physiologically relevant media (**Figure 1**). [12] By designing two meso-aryl free-base porphyrins with tailored electronic environments, one incorporating

View Article Online
DOI: 10.1039/D6MA00344C

electron-withdrawing cyano substituents, we demonstrate how rational molecular engineering can modulate solvation, aggregation behavior, excited-state rigidity, and overall photophysical performance. The probes exhibit a distinct dual optical response toward creatinine, arising from ground-state complexation and subsequent aggregate formation, enabling both chromogenic and fluorometric detection. [13] Importantly, the optimized probe maintains high sensitivity even in complex biological matrices such as diluted human urine, with minimal matrix interference, underscoring its practical relevance. These findings not only illuminate the structure–function relationship governing porphyrin–creatinine interactions but also establish a robust supramolecular platform with strong potential for developing low-cost, real-time, point-of-care diagnostic tools for renal health assessment. [14]

RESULTS AND DISCUSSION

Design Rationale and Synthesis Strategy of Probe Molecules: The design of Probes **1** and **2** was based on constructing a free-base meso-aryl porphyrin framework capable of forming well-defined hydrogen-bonding interactions with biomolecules. Porphyrin macrocycles are particularly attractive for sensing applications due to their strong absorption in the visible region, intense far-red fluorescence, and the presence of two inner pyrrolic N–H groups that serve as excellent hydrogen-bond donors. [15] To modulate the electronic and aggregation behaviour of the macrocycle, two meso-phenyl substituents were introduced, a cyano-substituted phenyl ring for Probe **1** and an unsubstituted phenyl ring for Probe **2**. The –CN groups in Probe 1 were incorporated to withdraw electron density from the macrocycle, enhance solvation in aqueous media, suppress aggregation, and stabilize the excited state, features that collectively improve fluorescence output and sensing sensitivity. [16] Both probes were synthesized through a classical acid-catalyzed condensation of the corresponding benzaldehyde derivative (R–C_6H_4–CHO) with pyrrole, followed by oxidative aromatization to furnish the fully conjugated porphyrin macrocycle. This modular synthetic approach allows substituent-controlled tuning of the electronic environment of porphyrin ring without altering the core structure responsible for binding events. [17] The structural features of these probes are highly relevant for the detection of creatinine. Creatinine contains both carbonyl and imine functionalities that act as strong hydrogen-bond acceptors, making it an ideal target for coordination with the inner N–H donors of the porphyrin. The presence of –CN groups in Probe 1 further strengthens this interaction by increasing the acidity of the core N–H protons and promoting formation of a more stable hydrogen-bonded complex. This complexation is expected to perturb the macrocyclic electronic structure, induce aggregation, and result in changes in optical behavior. [18] To further characterize Probe **1**, ^{1}H NMR and HRMS analyses were performed to confirm its structural integrity and molecular composition. (SEE ESI, Figure S1, S2 & S3.)

View Article Online
DOI: 10.1039/D6MA00344C

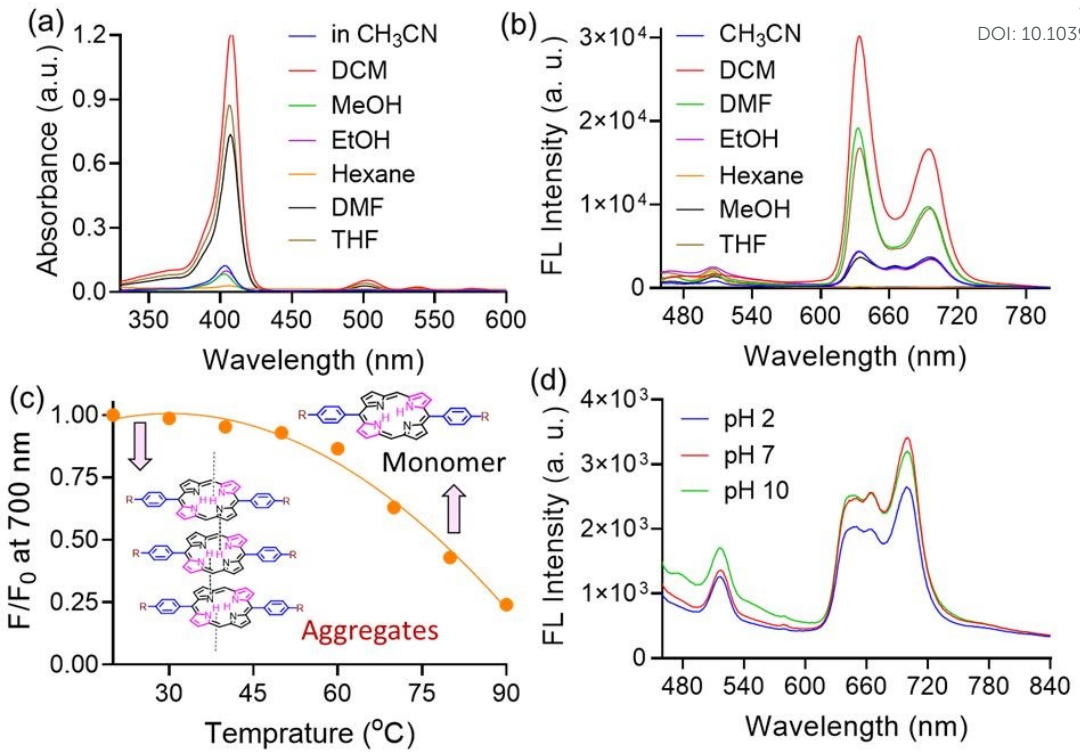

Figure 2. (a) UV-visible spectra of probe **1** (10 μM) in different organic solvents and water medium. (b) Fluorescence spectra of probe **1** (10 μM, λex = 430 nm) in different organic solvents and water medium. (c) Changes in fluorescence intensity of probe **1** (10 μM, λ_{ex} = 430 nm) at 700 nm at different temperature in the aqueous medium. (d) Fluorescence spectra of probe **1** (10 μM, λ_{ex} = 430 nm) in buffered medium at different pH conditions.

Investigation of Solvatochromic Responses: At first, we investigated the optical properties of the compound across a wide range of organic solvents and in aqueous medium. In relatively non-polar or moderately polar aprotic solvents such as DCM, THF, and DMF, the absorption spectra were dominated by sharp and highly intense Soret bands in the 400–430 nm region (**Figure 2a**). Under these conditions, the porphyrin remains predominantly in its well-solvated monomeric form, giving rise to narrow, well-resolved electronic transitions. [19] In contrast, in more polar and hydrogen-bonding solvents such as acetonitrile, ethanol, and methanol, the Soret bands became noticeably broader and exhibited significantly reduced molar absorptivities. A similar trend was observed in the Q-band region: three distinct bands centred at approximately 500, 535, and 575 nm were clearly resolved in DCM, THF, and DMF, whereas in the other solvents these features became broadened, partially merged, and markedly less intense. [20] The fluorescence spectra of the compound displayed two characteristic emission maxima at 634 and 695 nm (λex = 430 nm). Intense and well-defined emission bands were recorded in DMF, THF, and DCM, while protic solvents such as ethanol, methanol, and water produced significantly broadened and low-intensity emission profiles (**Figure 2b**). These pronounced solvent-dependent variations can be rationalized by multiple contributing factors. Increased solvent polarity stabilizes low-lying charge-transfer or dipole-enhanced excited states within the porphyrinic framework, leading to band broadening, weakened oscillator strengths, and reduced fluorescence. [21] In addition, protic solvents are capable of hydrogen bonding with the inner N–H groups of the macrocycle, perturbing its electronic distribution and promoting non-radiative decay pathways. In poor or strongly interacting solvents, partial π–π stacking or aggregate formation is also likely; such aggregation further broadens both the Soret and Q-bands and diminishes their intensities

View Article Online
DOI: 10.1039/D6MA00344C

through exciton coupling and reduced monomeric absorption. Collectively, these effects account for the decreased sharpness and diminished emission efficiencies observed in polar and protic media. [22]

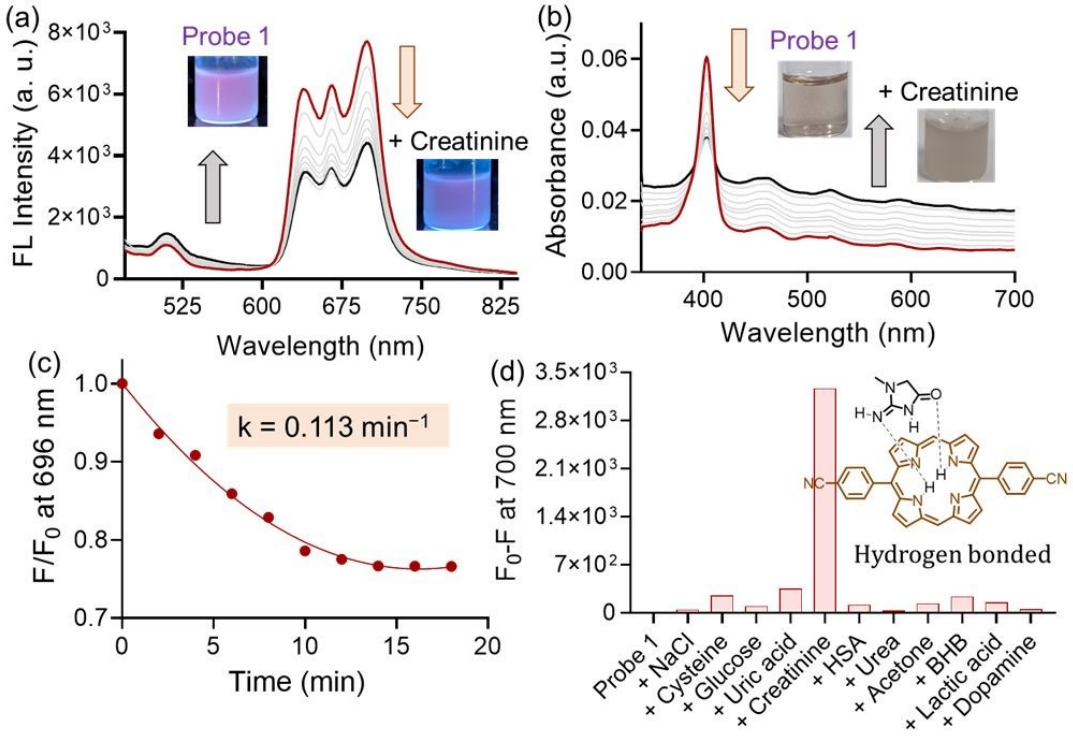

Figure 3. (a) Fluorescence titration of probe **1** (10 μM, λex = 430 nm) with creatinine (0 – 50 μM) in pH 7 buffered medium (b) UV-visible titration of probe **1** (10 μM) with creatinine (0 – 50 μM) in pH 7 buffered medium.(c) Changes in fluorescence intensity of probe **1** (10 μM, λex = 430 nm) at 700 nm with creatinine (50 μM) at room temperature in pH 7 buffered medium. (d) Changes in fluorescence intensity of probe **1** (10 μM, λex = 430 nm) upon addition of various analytes (50 μM) in pH 7 buffered medium.

Investigation of Stimuli-Responsive Behavior: To further understand the behaviour of the compound in aqueous medium, we examined its fluorescence response as a function of temperature and pH. Factors such as thermal fluctuations, protonation state of pyrrolic nitrogens, and aggregation dynamics govern the observed emission behaviour, making the compound a potential candidate for stimuli-responsive photophysical applications. The temperature-dependent spectral analysis showed that the fluorescence intensity at the principal emission maximum (λem ≈ 640 nm) systematically decreased with increasing temperature. At lower temperatures (10–20 °C), the emission remained relatively strong, whereas a gradual decline was observed from 30 °C onwards, ultimately resulting in a marked quenching at elevated temperatures (50–60 °C). This trend can be attributed to thermally assisted non-radiative decay; wherein higher thermal energy promotes vibrational relaxation and increases internal conversion rates (**Figure 2c**). [23] Moreover, elevated temperature can partially disrupt weak supramolecular interactions or enhance transient aggregation in water, both of which further reduce the fluorescence quantum yield. On the other hand, the pH-dependent fluorescence measurements revealed pronounced changes in emission behaviour across acidic, neutral, and alkaline conditions. Under neutral conditions (pH 7), the compound exhibited its characteristic dual emission peaks with moderate intensity. At acidic pH (pH 4), a slight decrease in fluorescence intensity was observed, although the overall emission profile remained largely

View Article Online
DOI: 10.1039/D6MA00344C

unchanged. This reduction can be attributed to protonation of the inner pyrrolic nitrogen atoms and peripheral basic sites, which perturbs the macrocycle's electronic structure and increases non-radiative decay efficiency (**Figure 2d**). Protonation decreases the aromatic stabilization of the porphyrin core and favours the formation of non-emissive protonated species, thereby lowering the radiative rate constant. In addition, protonation reduces the rigidity of the π-framework by modifying electron density and enhancing vibrational relaxation pathways, which further contributes to fluorescence quenching. [24]

Dual-Mode Response Towards Creatinine in Solution: To evaluate the chromogenic behaviour of probe **1** toward biologically relevant urinary biomarkers, we initially screened a panel of analytes including cysteine, albumin, uric acid, glucose, urea, β-hydroxybutyrate (BHB), acetone, lactic acid, creatine, dopamine, and others (**Figure 3d & S4**). Among all analytes tested, creatinine produced the most prominent optical response. Upon incremental addition of creatinine, the Soret band of probe **1** underwent a distinct hypochromic shift accompanied by substantial broadening, with the absorbance ratio A/A_0 decreasing ~2.2-fold at 402 nm (**Figure 3b**). [25] This attenuation indicates a strong ground-state interaction between creatinine and the porphyrinic macrocycle, most likely mediated through hydrogen bonding involving its carbonyl and imine groups. Such interactions perturb the π-electron distribution, weaken delocalization, and promote formation of loosely associated aggregated species, collectively reducing the oscillator strength of the Soret transition. In parallel, the UV–Vis spectra showed a noticeable increase in baseline intensity along with enhanced scattering in the longer wavelength region (>500 nm). This behavior indicates aggregate-induced light scattering arising from the formation of supramolecular probe–creatinine clusters in aqueous medium. The gradual baseline elevation at higher creatinine concentrations is attributed to the generation of larger aggregates or colloidal species, which might increase light scattering and influence the overall absorbance profile.[26] The fluorescence titration of Probe **1** with creatinine revealed a clear and concentration-dependent quenching effect (**Figure 3a**). The characteristic emission bands of the porphyrin (λ_{em} ~ 650–750 nm) decreased progressively (~1.8-fold) without significant alteration in spectral shape, confirming that the emissive framework remained intact, but its radiative efficiency was markedly reduced. Additionally, we have calculated the binding constants of Probe **1** and Probe **2** toward creatinine in aqueous medium using the Benesi–Hildebrand method. The calculated binding constant for Probe **1** was $K_b = 1.25 \times 10^4\ M^{-1}$, while Probe **2** exhibited a binding constant of $K_b = 4.154 \times 10^3\ M^{-1}$. This also confirms the higher quenching ability of probe 1 towards **(Figure S6 & S7**). Visually, the bright pink fluorescence of the probe under UV light gradually diminished and eventually became weak at higher creatinine concentrations. This quenching arises from creatinine–porphyrin interactions that perturb the excited-state electronic distribution and introduce efficient non-radiative decay channels.[27] The creatinine-induced aggregation observed in the absorption studies further contributes to quenching by generating non-emissive aggregate states through exciton coupling. Interestingly, the time-dependent fluorescence study of Probe **1** in the presence of creatinine showed a gradual decline in emission intensity, following a pseudo–first-order decay with a rate constant of $k = 0.113\ min^{-1}$. The fluorescence decreased rapidly during the initial minutes and gradually approached a steady state, indicating progressive formation of a less emissive probe–creatinine complex (**Figure 3c**). This kinetic behaviour suggests that creatinine undergoes a time-dependent association with the porphyrin, likely initiated by hydrogen bonding to the pyrrolic core, followed by slow reorganization into aggregated or microclustered species that strongly promote non-radiative decay. The evolution of these aggregated states accounts for the continuous quenching observed over time. [28]

View Article Online
DOI: 10.1039/D6MA00344C

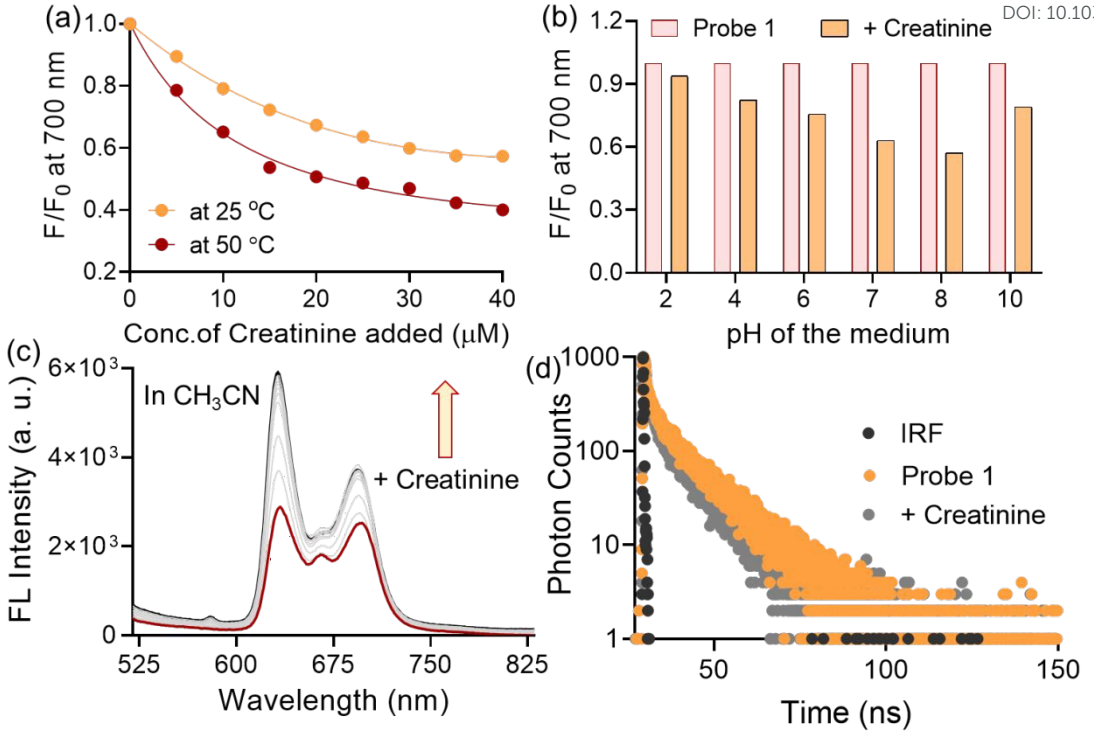

Figure 4. (a) Changes in fluorescence intensity of probe **1** (10 μM, λex = 430 nm) with creatinine (0 – 50 μM) at 25 and 50 °C in pH 7 buffered medium. (b) Changes in fluorescence intensity of probe **1** (10 μM, λex = 430 nm) with creatinine (50 μM) at different pH in buffered medium. (c) Fluorescence titration of probe **1** (10 μM, λex = 430 nm) with creatinine (0 - 50 μM) in CH_3CN. (d) Fluorescence decay profile of probe **1** (10 μM, λex = 430 nm) at 695 nm with and without creatine (50 μM) in pH 7 buffered medium.

Effects of Microenvironment on Recognition of Creatinine: The influence of temperature on the fluorescence response of Probe **1** toward creatinine was evaluated at two different temperatures, 25 °C and 50 °C (**Figure 4a**). The normalized fluorescence ratio (F/F_0 at 700 nm) decreased progressively with increasing creatinine concentration at both temperatures, but the extent of quenching was markedly greater at 50 °C (~2.5-fold). Elevated temperature enhances molecular diffusion and facilitates faster probe–creatinine association, while simultaneously increasing non-radiative decay pathways due to greater thermal agitation of the porphyrin framework. [29] These effects collectively promote more efficient excited-state deactivation, resulting in stronger quenching at higher temperature. The enhanced quenching at elevated temperature also suggests that the process has a significant dynamic component, since dynamic (collisional) quenching typically becomes more efficient with increasing temperature; however, the concurrent evidence of aggregation and ground-state complex formation indicates that static quenching may also contribute, implying that the overall quenching mechanism is likely a combination of both processes. [30]

Further, we investigated effect of pH on the emission response of **1** towards creatinine. The creatinine-treated samples consistently showed reduced F/F_0 values compared to **1** at all pH conditions, confirming that the quenching interaction is robust throughout the physiologically relevant pH window (**Figure 4b**). The modest enhancement in quenching efficiency near neutral to mildly basic pH (~7–9) can be rationalized by considering the acid–base properties of both the porphyrin core and creatinine. Free-base porphyrins contain four inner nitrogens: two pyrrolic

View Article Online
DOI: 10.1039/D6MA00344C

N–H donors, and two "imine-like" nitrogens whose lone pairs are part of the aromatic 18π system. All four nitrogens remain unprotonated across pH 2–10 because porphyrin core protonation requires strong mineral acids, not typical buffer acidity. [31] Thus, the two N–H groups retain full hydrogen-bond–donor character throughout this pH range. Creatinine, on the other hand, exhibits a protonation equilibrium around $pK_a \approx 4.8$; above this pH it exists largely in its neutral form, in which the carbonyl and imine sites behave as strong H-bond acceptors. Consequently, at neutral to mildly basic pH, where creatinine is mostly neutral and the porphyrin N–H donors are fully available, H-bond–driven binding is maximized, promoting ground-state association and aggregation that enhance non-radiative decay pathways. At more acidic pH, partial protonation of creatinine diminishes its H-bond–acceptor strength, slightly weakening complex formation and explaining the subtle pH dependence seen in the normalized quenching response. [32]

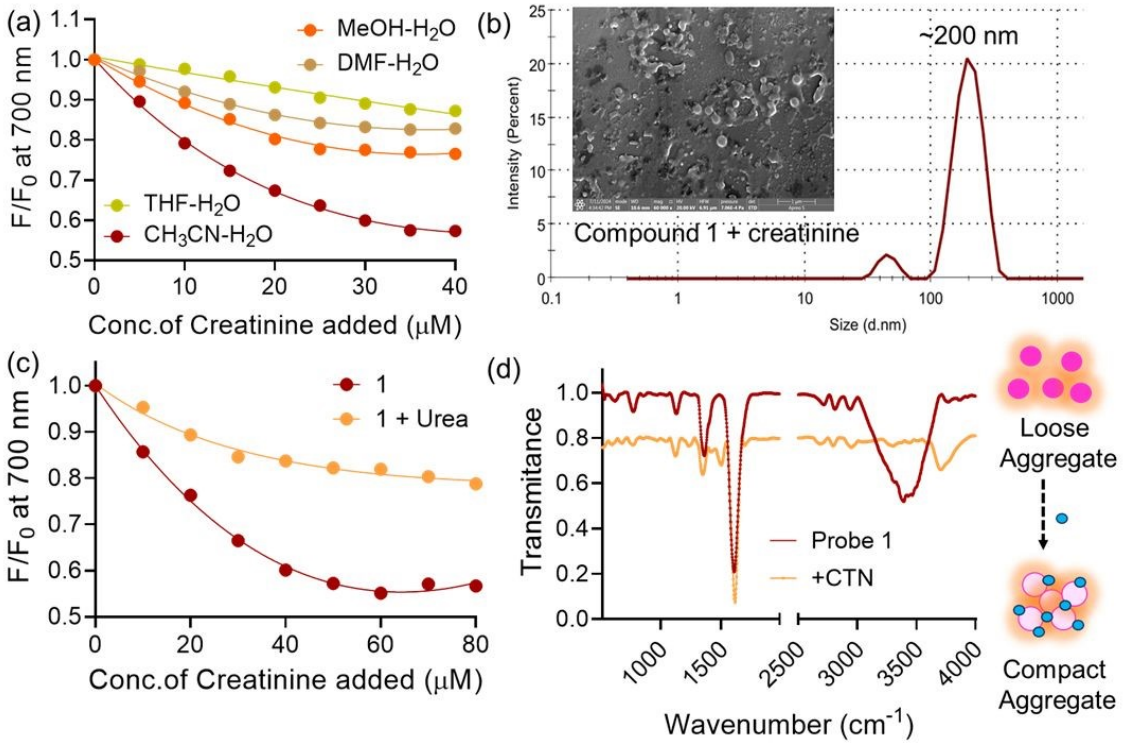

Figure 5. (a) Changes in fluorescence intensity of probe **1** (10 μM, λex = 430 nm) with creatinine (0 – 50 μM) in different organic-water mixture medium. (b) FESEM image and DLS of probe **1** with creatinine in pH 7 buffered medium. (c) Changes in fluorescence intensity of probe **1** (10 μM, λex = 430 nm) upon addition of creatinine (0 - 50 μM), both in the presence and absence of urea (5 M). (d) FT-IR spectra of **1** with creatinine.

Then we examined whether the solvent nature affected creatinine detection. For this purpose, acetonitrile, a polar aprotic solvent, was selected as an alternative medium. Interestingly, when Probe **1** was exposed to creatinine in acetonitrile, a turn-on fluorescence response (~1.5-fold enhancement) was observed (**Figure 4c**). This behaviour contrasts sharply with the quenching observed in aqueous medium and might be attributed to differences in solvation, hydrogen-bonding capacity, and aggregation propensity between the two solvents. The enhanced fluorescence observed in acetonitrile likely reflects a combination of improved solvation, reduced water-induced quenching, and suppression of non-radiative relaxation pathways in a polar aprotic medium.[33] Because acetonitrile lacks a strong hydrogen-bond-donating ability, it minimises solvent competition and can stabilise the emissive monomeric form of the probe. While

View Article Online
DOI: 10.1039/D6MA00344C

solvent-dependent changes in aggregation behavior may also contribute, the aggregation-driven emission enhancement is considered secondary to solvation and microenvironment effects. The time-resolved fluorescence data indicate that probe **1** exhibits a longer excited-state lifetime(~ 8.54 ns) in the absence of creatinine, whereas the lifetime becomes shorter upon addition of creatinine(~ 6.85 ns). This lifetime shortening is consistent with the formation of a probe–creatinine complex, where creatinine binding perturbs the local electronic environment of the porphyrin core, facilitating faster excited-state deactivation through aggregate-assisted relaxation processes (**Figure 4d**). Realizing the dominant role of solvent in governing the interaction between Probe **1** and creatinine, we further evaluated the fluorescence response in a series of mixed solvent systems comprising 50% (v/v) water and an organic co-solvent (THF, MeOH, DMF, or CH_3CN). Among these, the most pronounced response was observed in the CH_3CN–H_2O mixture, followed by CH_3OH–H_2O, DMF–H_2O, and THF–H_2O systems (**Figure 5a**). This trend reflects the combined influence of solvent polarity, hydrogen-bonding capability, and aggregation propensity on the sensing behaviour. In CH_3CN–H_2O, the polarity is sufficiently high to support strong porphyrin–creatinine association, while the limited hydrogen-bonding ability of acetonitrile helps suppress extensive porphyrin aggregation, thereby enhancing the fluorescence response. In contrast, protic or strongly coordinating solvents such as MeOH and DMF partially compete with creatinine for hydrogen bonding to the porphyrin N–H groups, reducing the effective binding interaction (**Figure 5b**). THF–H_2O, being less polar and less capable of stabilizing the porphyrin–creatinine complex, showed the weakest response. [34]

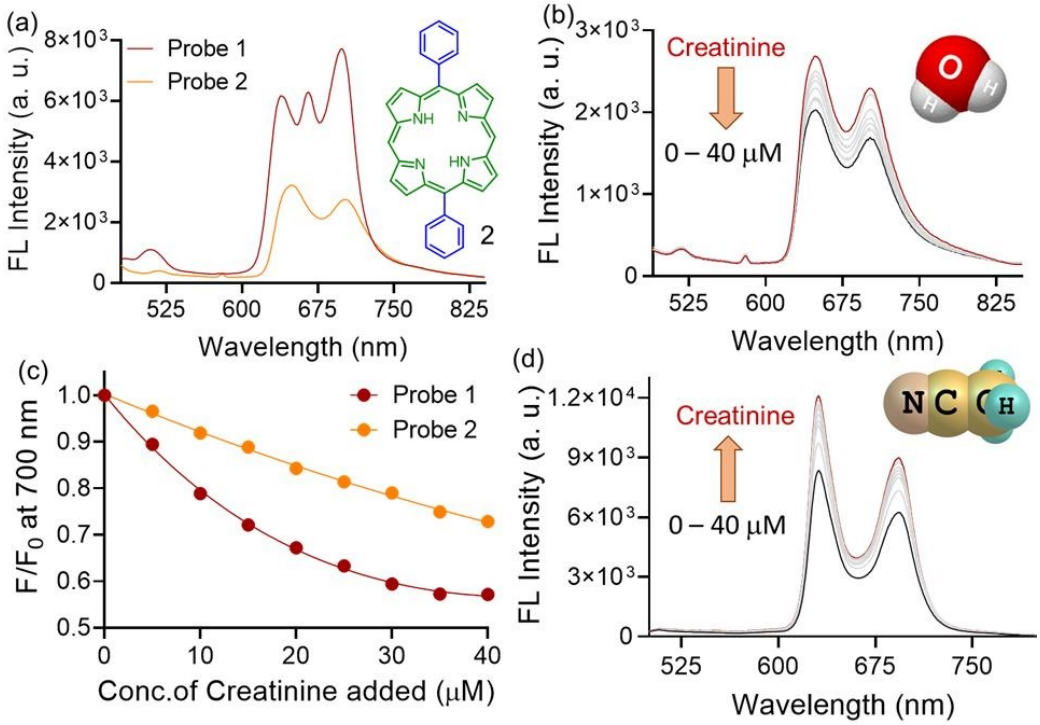

Figure 6. (a) Fluorescence spectra of probes **1** and **2** (10 μM) in pH 7 buffered medium. Fluorescence titrations of probe **2** (10 μM, λex = 430 nm) with creatinine (0 – 50 μM) (b) in pH 7 buffered medium (d) in CH_3CN medium. (c) Changes in fluorescence intensities of probes **1** and **2** (10 μM, λex = 430 nm) at 700 nm with creatinine (50 μM) in pH 7 buffered medium.

Mechanistic Investigation-Hydrogen Bonding with Creatinine: To examine potential interference from structurally related urinary metabolites, the fluorescence response of Probe **1**

View Article Online
DOI: 10.1039/D6MA00344C

toward creatinine was recorded in the presence of urea. In a typical experiment, the titrations of **1** with creatinine were performed both in the presence and absence of urea (5 M), and the changes in fluorescence responses (F/F_0) at 700 nm were noted. Interestingly, it was observed that the quenching efficiency was significantly reduced in samples pre-treated with urea (**Figure 5c**). This attenuation of the quenching effect indicates that urea partially suppresses the interaction between the probe and creatinine. Urea contains two carbonyl-associated $-NH_2$ groups capable of forming multiple hydrogen bonds with the porphyrin N–H donors, thereby occupying or competing for the same H-bonding/association sites that creatinine uses for complex formation. [35] As a result, creatinine binding becomes less efficient, leading to a diminished decrease in fluorescence intensity. Importantly, urea itself does not induce quenching, which confirms that the reduced response arises from competitive binding rather than probe destabilization. These findings demonstrate that while the probe retains selectivity for creatinine, strong hydrogen-bonding interferents such as urea can modulate binding efficiency through competitive site occupation. Further, the hydrogen bonding interaction between **1** and creatinine was confirmed by FT-IR studies (**Figure 5d**). The most prominent change was observed at higher energy region, where the N–H stretching band was found to be shifted from 3368 to 3296 cm^{-1} (Δ = 72 cm^{-1}), a magnitude that is fully consistent with the formation of moderately strong N–H…O/N hydrogen bonds, whereby coordination of carbonyl or imine functionalities of creatinine weakened the porphyrin N–H bond and lowers its vibrational frequency. The accompanying shift of the macrocyclic C=C/C=N skeletal vibration from 1616 to 1595 cm^{-1} reflected a subtle redistribution of π-electron density across the porphyrin framework upon hydrogen-bond engagement at the core. Likewise, the blue shift in the pyrrole-based C–N/C–C in-plane modes (1357 → 1336 cm^{-1}) indicated the local perturbation of the pyrrolic subunits due to complexation. Together, these correlated shifts and the associated band broadening provide strong spectroscopic evidence that creatinine forms a hydrogen-bonded adduct with the porphyrin core, inducing measurable structural and electronic changes consistent with the optical responses observed in UV–Vis and fluorescence studies. [36] Further, we have also recorded the FT-IR spectrum of **1** with acid under similar conditions. Acid addition caused the shifting of the broad O-H/N-H stretching peak from 3377 cm^{-1} to 3428 cm^{-1}, indicating possible protonation interaction. (**Figure S5**) The formation of Probe **1** with creatinine adduct was further confirmed by high-resolution mass spectrometry (HRMS) analysis. A new peak was observed at m/z 625.18 corresponding to the molecular ion peak [$C_{38}H_{27}N_9O$] (**Figure S3**). Further, the Dynamic light scattering (DLS) and SEM analyses confirmed the creatinine-promoted aggregation of probe **1** in the aqueous medium. The DLS studies with **1** alone displayed a narrow size distribution of hydrodynamic diameter centred around ~160 nm, consistent with the formation of small, well-dispersed nanoaggregates. Upon addition of creatinine, however, the hydrodynamic diameter increased substantially to ~200 nm, accompanied by the appearance of a secondary population at smaller sizes (~50 nm), indicating heterogeneous aggregation. Temperature-dependent (40-60˚C) DLS showing a gradual size decrease for probe **1** from 150 ± 8 nm to 89 ± 7 nm with increasing temperature, indicating thermal disassembly of aggregates into compact monomers. (**Table T1**) The SEM images likewise revealed the transition from relatively discrete nanoscale assemblies in the free probe to more densely packed and irregularly fused clusters in the creatinine-treated sample. This increase in aggregate size can be attributed to hydrogen-bond-driven association between the porphyrin N–H groups and the carbonyl/imine functionalities of creatinine, which promotes interparticle bridging and facilitates growth of larger supramolecular structures. [37]

View Article Online
DOI: 10.1039/D6MA00344C

Effects of Functional Groups on Creatinine Binding: Further, we investigated the electronic influence of substituents on the fluorescence responses of Probes **1** and **2** in aqueous medium (**Figure 6a**). Probe **1**, bearing –CN groups on both meso-phenyl rings, exhibited substantially stronger fluorescence than Probe **2**, which contains unsubstituted phenyl rings. This behaviour is attributed to the strong electron-withdrawing and resonance-stabilizing nature of the –CN groups. The cyano substituents decrease electron density on the meso-aryl units and, through conjugation, modulate the electronic distribution of the porphyrin macrocycle. Such electronic withdrawal (i) stabilizes the excited singlet state, (ii) suppresses non-radiative decay pathways, and (iii) reduces aggregation-induced quenching by enhancing solvation and weakening intermolecular π–π interactions in water. [38] As a result, Probe **1** sustains a larger population of radiatively decaying excited states and therefore displays higher fluorescence intensity. In contrast, Probe **2** lacks electron-withdrawing substituents, leaving the porphyrin framework more electron-rich and more prone to π–π-driven aggregation in aqueous medium (**Figure 6b & d**). This is consistent with DLS measurements, which show that Probe **2** forms significantly larger colloidal nanoaggregates (average hydrodynamic diameter ~270–280 nm), a regime known to facilitate exciton coupling and enhance non-radiative decay, leading to reduced fluorescence. Upon exposure to creatinine, Probe **2** displayed ~1.34-fold quenching of fluorescence intensity, slightly weaker than that observed with Probe **1**, suggesting a similar but less efficient interaction (**Figure 6c**). Interestingly, Probe **2** also exhibited a creatinine-induced turn-on response in mixed solvent conditions, indicating that, despite its stronger aggregation tendency in pure water, it retains the ability to undergo excited-state rigidification or disaggregation upon creatinine binding under appropriate solvation environments (**Figure 7a**). [39]

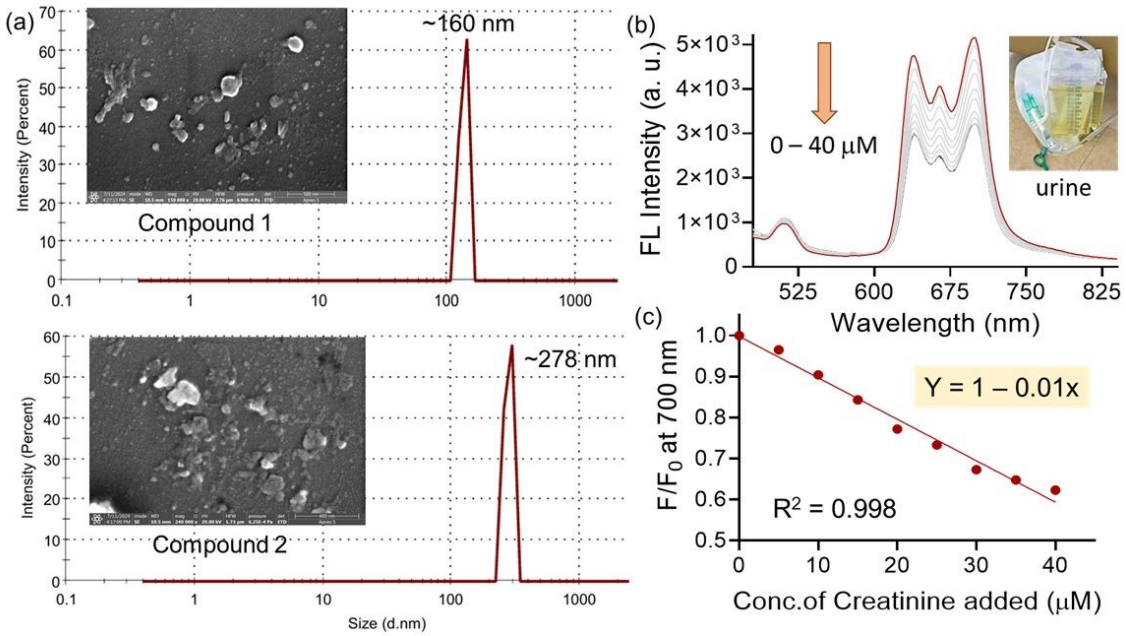

Figure 7. (a) FESEM images and DLS of probes **1** and **2** at pH 7 in buffered medium. (b) Fluorescence titration of probe **1** (10 µM, λex = 430 nm) with creatinine (0 – 40 µM) in diluted urine (10 % in pH 7 buffered medium). (c) Changes in fluorescence intensity of probe **1** (10 µM, λex = 430 nm) at 700 nm with creatinine (40 µM) in diluted urine (10 % in pH 7 buffered medium).

Semiquantitative Fluorimetric Assay in Urine Samples: The ability to determine creatinine levels in urine is clinically valuable, as urinary creatinine serves as a key biomarker for kidney

View Article Online
DOI: 10.1039/D6MA00344C

function, glomerular filtration efficiency, and metabolic status. Accurate and rapid measurement of creatinine is essential for diagnosing renal disorders, monitoring chronic kidney disease progression, and assessing overall physiological well-being. [40] Considering the excellent sensitivity of probe **1** toward creatinine, we further explored its applicability for detecting creatinine in real biological samples. Freshly collected human urine from a healthy volunteer was diluted to 10% (v/v) in buffered medium and subjected to fluorescence measurement. The emission spectrum of probe **1** in the diluted urine sample showed no appreciable changes in intensity or spectral profile compared to that recorded in buffer alone, indicating that common urinary components do not interfere significantly with the photophysical behavior of the probe (**Figure 7b**). Upon spiking the urine sample with increasing concentrations of creatinine (0–40 μM), a clear and systematic quenching of fluorescence intensity was observed, amounting to ~1.62-fold decrease at the 700 nm emission band. Plotting the normalised fluorescence change against creatinine concentration yielded a linear response (Y = 1 – 0.01x) with an excellent correlation coefficient (>0.98), confirming that probe **1** can reliably quantify creatinine in complex biological matrices with minimal matrix effects (**Figure 7c**). [41] The present results demonstrate that probe **1** is capable of functioning as a practical fluorescence-based platform for creatinine detection in real urine samples, highlighting its translational potential for point-of-care or routine clinical screening.

CONCLUSION

In summary, this work establishes meso-aryl free-base porphyrins as an effective supramolecular platform for the optical detection of creatinine through hydrogen-bond–mediated ground-state complexation. The incorporation of electron-withdrawing –CN substituents in Probe **1** significantly enhances photostability, solvation, and excited-state rigidity, resulting in reduced aggregation and superior fluorescence performance relative to the unsubstituted analogue. Comprehensive spectroscopic analyses, including UV–Visible titration, steady-state and time-resolved fluorescence, FT-IR, DLS, and SEM, collectively validate that creatinine binding induces pronounced hypochromicity, far-red emission quenching, and formation of larger supramolecular aggregates. These effects arise from N–H···O/N hydrogen bonding between the porphyrin core and the carbonyl/imine functionalities of creatinine, which perturb the macrocyclic π-framework and promote non-radiative decay channels. Importantly, Probe **1** demonstrates robust sensing across varying microenvironments and enables semi-quantitative detection of creatinine in diluted human urine with excellent linearity and minimal matrix interference, underscoring its translational potential for point-of-care renal biomarker monitoring.

ACKNOWLEDGEMENT

KS acknowledges the DST–INSPIRE Fellowship, Department of Science and Technology, Government of India, for financial support during this PhD research. ND and AP thank ICMR for research grants (ITR/ 2021-8350). The authors thank BITS Pilani Hyderabad for technical help.

REFERNCES

1. R. Paolesse, S. Nardis, D. Monti, M. Stefanelli and C. Di Natale, Porphyrinoids for chemical sensor applications, *Chem. Rev.*, 2017, **117**(4), 2517–2583.

2. J. Huang, J. Li, Y. Lyu, Q. Miao and K. Pu, A self-assembled semiconducting polymer nanoassembly for second near-infrared photothermal therapy, *Nat. Mater.*, 2019, **18**(10), 1133–1143.
3. Y. He, H. Wang, C. He, R. Zeng, F. Cheng, Y. Hao, P. Zhang *et al*., A porphyrin-based colorimetric and near infrared fluorescent probe for reversible and rapid detection of diethyl chlorophosphate, *Sens. Actuators, B*, 2025, **425**, 136983.
4. S. Arora, R. Nagpal, M. Gusain, B. Singh, Y. Pan, D. Yadav and B. Parshad, Organic–inorganic porphyrinoid frameworks for biomolecule sensing, *ACS Sens.*, 2023, **8**, 443–452.
5. M. Kielmann and M. O. Senge, Molecular engineering of free-base porphyrins as ligands—The N–H···X binding motif in tetrapyrroles, *Angew. Chem. Int. Ed.*, 2019, **58**(2), 418–441.
6. X. Huang, Y. Zhou, Y. Zeng, X. Chen, F. He, T. Wang, P. Gao *et al*., Electron-donating/withdrawing groups functionalized porphyrin complex as high-performance organic lithium batteries, *Chem. Eng. J.*, 2023, **470**, 144248.
7. Z. X. Qin, C. Y. Wang, J. S. Zhang, Z. Y. Wang, Y. Wei, Y. T. Li and L. N. Niu, DNA-Based Materials Inspired by Natural Extracellular DNA, *Adv. Funct. Mater.*, 2023, **33**, 2211669.
8. S. Mondal, I. Ahmad, and N. Dey, Multifaceted Applications of Luminescent Metalloporphyrin Derivatives: Fluorescence Turn-On Sensing of Nicotine and Antimicrobial Activity. ACS Appl. Bio Mater., 2024, 7, 2346–2353.
9. J. Hwang, T. S. Reddy, H. Moon, H. D. Lee and M. S. Choi, Cyanide detecting porphyrin fluorescent sensors: Effects of electron-donating/withdrawing substituents, *Dyes Pigm.*, 2023, **215**, 111243.
10. L. Jiang, Y. Imanaka and H. Fujii, Tuning catalytic activity with steric and electron-withdrawing effects of a porphyrin substituent, *Catal. Sci. Technol.*, 2023, **13**, 5280–5289.
11. R. S. Fernandes, A. Tiwari, S. Kanungo and N. Dey, Formation of Stable Naphthalenediimide Radical Anion: Substituent-Directed Synergetic Effects of Hydrogen Bonding and Charge Transfer Interactions on Chromogenic Response Towards Hydrazine, *J Mol Liq*., 2023, **387**, 122238.
12. A. Zhang, L. Kwan and M. J. Stillman, The spectroscopic impact of interactions with the four Gouterman orbitals from peripheral decoration of porphyrins with simple electron-withdrawing and donating groups, Org. Biomol. Chem., 2017, 15(43), 9081–9094.
13. Mondal, S., Pain, T., Sahu, K., & Kar, S. Large-scale green synthesis of porphyrins. *ACS omega*,2021, **6**(35), 22922-22936.
14. H. Lee, H. Park, D. Y. Ryu and W. D. Jang, Porphyrin-based supramolecular polymers. Chem. Soc. Rev., 2023, **52**(6), 1947–1983.
15. A. Antoniuk-Pablant, Y. Terazono, B. J. Brennan, B. D. Sherman, J. D. Megiatto, G. W. Brudvig, A. L. Moore, T. A. Moore and D. Gust, A new method for the synthesis of β-cyano substituted porphyrins and their use as sensitizers in photoelectrochemical devices, *J. Mater. Chem. A*, 2016, **4**(8), 2976–2985.
16. S. Francis, N. Sunny and L. Rajith, Picomolar selective fluorescent detection of creatinine using porphyrin in aqueous medium, *J. Photochem. Photobiol. A: Chem.*, 2023, **438**, 114534.
17. N. Amiri, M. Guergueb, A. Haouas, M. Bourguiba and H. Nasri, Bis (DMAP) cobalt (II) porphyrin complexes: Dielectric properties and visible light irradiated photocatalytic degradation of toluidine blue studies. Inorg. Chem. Commun., 2023, **158**, 111551.
18. B. Chettri, S. Jha, and N. Dey, Unique CT emission from Aryl Terpyridine Nanoparticles in Aqueous Medium: A Combined Effect of Excited State Hydrogen bonding and Conformational Planarization, *J. Photochem. Photobiol. A*, 2023, **435**, 114210.

View Article Online
DOI: 10.1039/D6MA00344C

19. Y. Gao, Y. Li, Z. Xu, S. Yu, J. Liu and H. Sun, Multiporphyrinic architectures: Advances in structural design for photodynamic therapy. Aggregate, 2024, **5**(2), e420.
20. G. Li, J. Du, Z. Wang, C. Ren, F. Lu and Q. Deng, Porphyrin based covalent organic polymer for the fluorescence sensing of water in organic solvents, *Dyes Pigm.*, 2024, **222**(1), 111924.
21. K. Prakash, M. Sankar, S. Seetharaman and F. D'Souza, Synthesis, electrochemical and photochemical studies on π-extended mono-β-functionalized porphyrin dyads, *ChemPhotoChem*, 2019, **3**(3), 151–165.
22. W. Suzuki, H. Kotani, T. Ishizuka, K. Ohkubo, Y. Shiota, K. Yoshizawa *et al*., Thermodynamics and photodynamics of a monoprotonated porphyrin directly stabilized by hydrogen bonding with polar protic solvents, *Chem. Eur. J.*, 2017, **23**(19), 4669–4679.
23. M. F. Mabesoone, A. J. Markvoort, M. Banno, T. Yamaguchi, F. Helmich, Y. Naito *et al*., Competing interactions in hierarchical porphyrin self-assembly introduce robustness in pathway complexity, *J. Am. Chem. Soc.*, 2018, **140**(25), 7810–7819.
24. M. Zannotti, R. Giovannetti, B. Minofar, D. Řeha, L. Plačková, C. A. D'Amato *et al*., Aggregation and metal-complexation behaviour of THPP porphyrin in ethanol/water solutions as function of pH, *Spectrochim. Acta, Part A*, 2018, **193**, 235–248.
25. S. Francis, N. Sunny and L. Rajith, Picomolar selective fluorescent detection of creatinine using porphyrin in aqueous medium, *J. Photochem. Photobiol. A: Chem.*, 2023, **438**(1), 114534.
26. Y. Zhao, Y. Hu, Y. Zhong, J. Wang, Z. Liu, F. Bai and D. Zhang, Missing links between the structures and optical properties of porphyrin assemblies, *J. Phys. Chem. C*, 2021, **125**(40), 22318–22327.
27. R. Teixeira, V. V. Serra, D. Botequim, P. M. Paulo, S. M. Andrade and S. M. Costa, Fluorescence spectroscopy of porphyrins and phthalocyanines: Some insights into supramolecular self-assembly, microencapsulation, and imaging microscopy, *Molecules*, 2021, **26**(14), 4264.
28. G. B. Bodedla, M. Imran, J. Zhao, X. Zhu and W. Y. Wong, Design of AIEgen-based porphyrin for efficient heterogeneous photocatalytic hydrogen evolution: Special Collection: Aggregation-Induced Processes and Functions, *Aggregate*, 2023, **4**(5), e364.
29. A. Vyšniauskas, D. Ding, M. Qurashi, I. Boczarow, M. Balaz, H. L. Anderson and M. K. Kuimova, Tuning the sensitivity of fluorescent porphyrin dimers to viscosity and temperature, *Chem. Eur. J.*, 2017, **23**(46), 11001–11010.
30. M. Venkatesan, H. Mandal, M. Chakali and P. R. Bangal, Excited-state quenching of porphyrins by hydrogen-bonded phenol–pyridine pair: Evidence of proton-coupled electron transfer, *J. Phys. Chem. C*, 2019, **123**(38), 23342–23351
31. Y. J. Hou, S. Fang, X. Y. Zhang, J. Wang, Q. Ruan, Z. Xiang and X. J. Zhu, ACS Appl. Mater. Interfaces, 2022, **14**(43), 49875–49884.
32. R. Jäger, M. Purpura, A. Shao, T. Inoue and R. B. Kreider, Analysis of the efficacy, safety, and regulatory status of novel forms of creatine, Amino Acids, 2011, **40**(5), 1369–1383
33. A. Singha, K. Mittra and A. Dey, Effect of hydrogen bonding on innocent and non-innocent axial ligands bound to iron porphyrins, Dalton Trans., 2019, **48**(21), 7179–7186.
34. A. Pal, I. Ahmad and N. Dey, Hydrogen-Bond-Assisted Dual-Mode Ratiometric Detection of Uric Acid Using Pyrimidine-Driven Charge Transfer Probes: From Mechanistic Studies to Real-Life Applications. ACS Appl. Bio Mater., 2025, **8**(7), 4699–4706.
35. N. Dey and S. Bhattacharya, Hydrogen bonding-induced unique charge-transfer emission from multi chromophoric polypyridyl ligands: ratiometric probing of methanol impurity in commercial biofuels, ACS Sustainable Chem. Eng., 2021, **9**(50), 17078–17084.

36. B. Chettri, A. Pal, S. Jha and N. Dey, Tuning sensing efficacy of anthraimidazoledione-based charge transfer dyes: nitro group positioning impact, *Dalton Trans.*, 2024, **53**(14), 6343–6351.
37. R. S. Fernandes and N. Dey, Exploring the synergistic effect of aggregation and hydrogen bonding: a fluorescent probe for dual sensing of phytic acid and uric acid, *J. Mater. Chem. B*, 2024, **12**(45), 11789–11799.
38. S. Patil, S. Pise and N. Dey, Tuneable charge-transfer probes for environmental monitoring: Phthalimide-linked pyrene-dione probes for ratiometric sensing of Cu^{2+}, *J. Mol. Struct.*, 2025, **1337**(1), 142103.
39. S. Mondal, S. Paul and N. Dey, Host–guest-mediated modulation of pyrimidine charge-transfer probes by cyclodextrin nanosponges for aqueous-phase cyanide detection, *Langmuir*, 2025, **41**(39), 26789–26797.
40. S. Ozdemir, C. G. Sears, J. M. Harrington, A. H. Poulsen, J. Buckley, C. J. Howe and J. Meliker, Relationship between urine creatinine and urine osmolality in spot samples among men and women in the Danish diet cancer and health cohort. *Toxics,* 2021, 9(11), 282.
41. A. Pal and N. Dey, A chromogenic anthraimidazoldione probe for ratiometric analysis of Hg2+ exclusively at mesoscopic interface: Screening of real-life biological samples. *Colloids Surf. A*, 2024, **687**, 133397.

Hydrogen-Bonding Mediated Supramolecular Assembly of Fluorescent Meso-Aryl Porphyrins for Creatinine Monitoring in Biological Samples

View Article Online
DOI: 10.1039/D6MA00344C

Karisma Sharma,[a] Animesh Pal,[b] Satadru Jha,[a] Nilanjan Dey[b*]
[a] Department of Chemistry, Sikkim Manipal Institute of Technology,
Sikkim Manipal University, Majitar, Sikkim 737136, India.
[b] Department of Chemistry, BITS-Pilani Hyderabad Campus, Shameerpet, Hyderabad-500078,
Telangana, India, *Email: nilanjandey.iisc@gmail.com

Data will be available from authors on reasonable request